

A Constrained Level Set Method for Simulating the Formation of Liquid Bridges

Dongdong He and Huaxiong Huang*

Department of Mathematics and Statistics, York University, Toronto, Ontario, Canada M3J 1P3.

Received 18 November 2010; Accepted (in revised version) 9 August 2011

Available online 20 February 2012

Abstract. In this paper, we investigate the dynamic process of liquid bridge formation between two parallel hydrophobic plates with hydrophilic patches, previously studied in [1]. We propose a dynamic Hele-Shaw model to take advantage of the small aspect ratio between the gap width and the plate size. A constrained level set method is applied to solve the model equations numerically, where a global constraint is imposed in the evolution [2] stage together with local constraints in the reinitialization [3] stage of level set function in order to limit numerical mass loss. In contrast to the finite element method used in [2], we use a finite difference method with a 5th order HJWENO scheme for spatial discretization. To illustrate the effectiveness of the constrained method, we have compared the results obtained by the standard level set method with those from the constrained version. Our results show that the constrained level set method produces physically reasonable results while that of the standard method is less reliable. Our numerical results also show that the dynamic nature of the flow plays an important role in the process of liquid bridge formation and criteria based on static energy minimization approach has limited applicability.

AMS subject classifications: 76T99, 65M06

Key words: Constrained level set method, Hele-Shaw, liquid bridges, mass conservation, moving interface.

1 Introduction

In recent years, rapid progresses have been made in miniature manufacturing and testing processes to take advantage of the increasing portable computing power. In [1], an experimental procedure is proposed for setting up a simple device for biomedical testing. By filling the gap between two parallel plates with a prepared solution and subsequent

*Corresponding author. *Email addresses:* ddonghe@yorku.ca (D. He), hhuang@yorku.ca (H. Huang)

formation of isolated liquid bridges between the plates, many tests can be preformed simultaneously. This was achieved by treating the two plates chemically to form circular hydrophilic patches and displacing the water-based solution with a non-immersible second fluid, e.g., silicon oil. A static model was used in [1] to predict the formation of these liquid bridges, by minimizing equilibrium surface energy. Since the formation of liquid bridges is a dynamic process, a more accurate model must go beyond the static approach.

In this paper, we adopt a dynamic Hele-Shaw model to take the advantage of the fact that the gap between the plates is small relatively to the size of the plates. And we use a level set method to numerically study the formation of liquid bridges between two patched surfaces. Furthermore, we investigate the effects of relevant physical parameters such as the viscosity ratio and capillary number, and our numerical results are consistent with those in the existing literature.

In our numerical computation, the interface between the two fluids is captured using a level set method while the Hele-Shaw equations are solved by a first order ghost fluid method [5][†]. The level set method is one of the widely used approaches for problems with evolving interfaces, especially when topological changes are involved [4]. The standard level set method uses the zero level set of a smooth scalar function (usually the signed distance function) to represent the interface. The evolution of the level set function is normally governed by a transportation equation, high order methods (ENO or WENO) can be easily applied. In order to maintain the level set function as a signed distance function, a reinitialization process is needed. Although it is easy to implement, the standard level set method suffers serious mass loss. As a consequence, for a divergence-free velocity field, the computed area (volume) enclosed by the zero level set usually does not stay as a constant.

The objective of our paper is twofold. Our main purpose is to assess the importance of the dynamic aspect of the liquid bridge process that is useful for designing miniature test devices with a wide range of applications. In order to make accurate predictions, maintaining mass conservation is crucial for this class of problems and an important objective of this study is to present a method that is easy to implement and capable of handling topological changes of a moving interface. This is achieved by using a constrained level set method. While the idea of using constraints in the level set approach is not new, we have made a number of improvements in the implementations. First of all, a global constraint is imposed in the evolution stage [2] together with local constraints in the reinitialization stage [3] of level set function in order to limit numerical mass loss. Secondly, in contrast to the low order finite element method [2], we use a 5th order HJWENO scheme for spatial discretization. As a result, our version of the constrained level set method is more accurate than the existing ones. Our numerical tests based on standard test problems show that a significant improvement is achieved. Having established the reliability of the numerical method, we carry out extensive numerical simulations of the liquid bridge

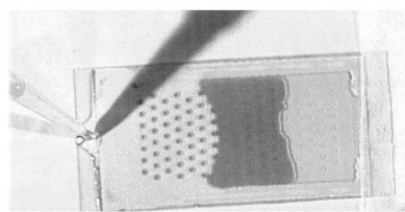
[†] Although high order methods such as a hybrid immersed interface level set method [6] could also be used, our focus here is to study the effect of the dynamics, and the current first order method is sufficiently accurate as long as certain precaution is taken.

formation process. Our simulations show that the prediction of a static surface energy minimizer has limited applicability. In general, the dynamic nature of the flow plays an important role in the formation process of liquid bridges.

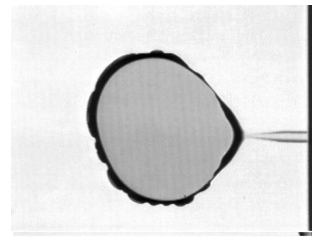
The rest of the paper is organized as follows. In Section 2 we present the basic mathematical model. A constrained level set method with a high order difference discretization (HJWENO) is given in Section 3. Numerical results are given in Section 4. A brief conclusion and discussion of future directions is given in Section 5. In Appendix B, we present comparisons between the standard and constrained level set methods using standard numerical tests, where we show that the HJWENO scheme produces much more accurate results than that of the finite element method [2].

2 Problem description

The experimental setup used in [1] is shown in Fig. 1(a), where two parallel plates are placed in close proximity. The sample solution (water) filled in the gap between the two plates is slowly displaced by another fluid. Since the circular patches (dark spots) are more hydrophilic compared to the rest, it is more difficult to displace water from these patches. Often, the displacing fluid removes most of the water in the gap except in the areas directly over the patches. The water over these patches form isolated liquid bridges immersed in the non-reacting fluid, as shown in Fig. 1(b).



(a) Displacing water (dark colored) by another fluid



(b) Close-up view of liquid bridge formation

Figure 1: An illustration of filling fluids and formation of the liquid bridge (reproduced from [1]).

We consider a simple case consisting of two parallel plates sized $[-1,1] \times [-1,1]$, and a circular patch centered at $(-0.5,0)$ with radius 0.25 on each plate. The circular patch is hydrophilic while the rest of the plates is hydrophobic. Both plates have the same wetting property for the fluids, a top view of the problem is given in Fig. 2. Furthermore, we assume that the aspect ratio of the device is sufficiently small, by lubrication theory, the two-phase flow can be modeled by the (non-dimensional) Hele-Shaw equations [5]

$$\vec{u} = \beta \nabla p, \quad (2.1)$$

$$\nabla \cdot \vec{u} = 0 \quad (2.2)$$

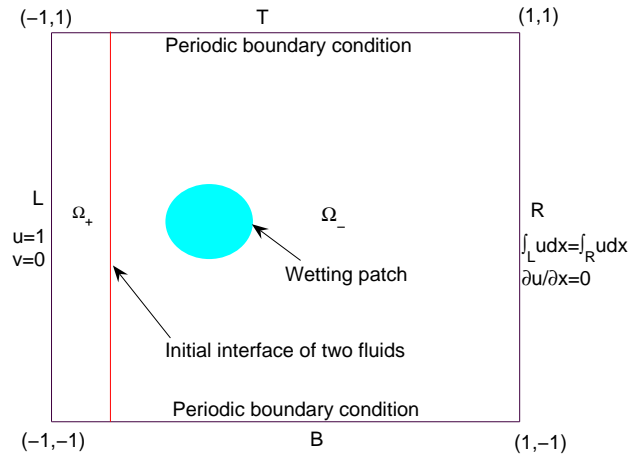


Figure 2: Computational domain and boundary conditions for liquid bridge formation process.

for \vec{x} in Ω_+ and Ω_- with jump conditions

$$[p] = \kappa_{xy} + \frac{\kappa_z}{\lambda}, \tag{2.3}$$

$$[\vec{u} \cdot \vec{n}] = [\beta \nabla p \cdot \vec{n}] = 0 \tag{2.4}$$

on Γ where

$$\beta = \begin{cases} \beta_+ \triangleq -\frac{\lambda^2}{12\eta Ca'}, & \vec{x} \in \Omega_+, \\ \beta_- \triangleq -\frac{\lambda^2}{12Ca'}, & \vec{x} \in \Omega_-. \end{cases} \tag{2.5}$$

Here $Ca = \frac{\mu_- U}{\sigma}$ is the capillary number, U is the characteristic velocity, λ is the aspect ratio, $\eta = \frac{\mu_+}{\mu_-}$ is the ratio of viscosities, κ_{xy} is the non-dimensional curvature in the xy plane, and

$$\kappa_z = -2\cos\theta \tag{2.6}$$

is the non-dimensional curvature in z direction under the assumption that the interface along z direction is a circular arc [5].

We use $u = 1, v = 0$ as the boundary condition on the left boundary L , and use the condition $\int_L u dx = \int_R u dx, \frac{\partial u}{\partial x} = 0$ on the right boundary R to ensure that global mass is conserved. Moreover, periodic boundary conditions are used on the top and bottom boundaries. We assume that the initial interface is a straight line parallel to y axis which is set to be $x = -0.9$ and the region occupied by the displaced fluid is Ω_- , while the region occupied by the displacing fluid is Ω_+ .

3 Numerical method

We apply the level set method to capture the interface between two fluids. For comparison purposes, we use both the standard and constrained formulations. We refer readers to [7] and [5] for detail description of the standard level set method. And we shall represent the constrained level set method as follows.

3.1 Constrained level set method

In [2], the authors propose the constrained method for the level set equation as

$$\phi_t + \vec{u} \cdot \nabla \phi + \lambda(t) = 0. \quad (3.1)$$

Here λ is the Lagrange multiplier, subjected to the following condition

$$\frac{d}{dt} \left(\int_{\Omega} H(\phi) dx \right) = 0, \quad (3.2)$$

where Ω is the computational domain, H is the Heaviside function. Substituting (3.1) into (3.2), we obtain

$$\lambda(t) = - \frac{\int_{\Omega} \vec{u} \cdot \nabla \phi \delta(\phi) dx}{\int_{\Omega} \delta(\phi) dx}. \quad (3.3)$$

In this paper, the delta function is regularized by

$$\delta_{\varepsilon}(\phi) = \begin{cases} 0, & \text{if } \phi < -\varepsilon, \\ \frac{1}{2\varepsilon} + \frac{1}{2\varepsilon} \cos\left(\frac{\pi\phi}{\varepsilon}\right), & \text{if } -\varepsilon \leq \phi \leq \varepsilon, \\ 0, & \text{if } \phi > \varepsilon. \end{cases} \quad (3.4)$$

The area enclosed by the zero contour of the level set function is calculated using integral $\int_{\Omega} H_{\varepsilon}(\phi) dx$, where H_{ε} is the regularized Heaviside function

$$H_{\varepsilon}(\phi) = \begin{cases} 0, & \text{if } \phi < -\varepsilon, \\ \frac{1}{2} + \frac{\phi}{2\varepsilon} + \frac{1}{2\pi} \sin\left(\frac{\pi\phi}{\varepsilon}\right), & \text{if } -\varepsilon \leq \phi \leq \varepsilon, \\ 1, & \text{if } \phi > \varepsilon. \end{cases} \quad (3.5)$$

In all the following computations, we use uniform meshes, and set $\varepsilon = 1.5h$, where h is the mesh size.

When the velocity field is divergence free, it is easy to show that $\lambda(t) \equiv 0$ [2]. However, in discrete form, this may not be the case. By choosing λ through (3.3), we can ensure mass conservation (3.2) in continuous form and improve mass conservation in discrete form. This is demonstrated as follows.

The discretization form of (3.1) is

$$\phi_{ij}^{n+1} - \phi_{ij}^n = \left[-\bar{u}_{ij}^n \cdot (\nabla \phi)_{ij}^n + \frac{\sum_{ij} \bar{u}_{ij}^n \cdot (\nabla \phi)_{ij}^n \delta_\varepsilon(\phi_{ij}^n)}{\sum_{ij} \delta_\varepsilon(\phi_{ij}^n)} \right] \Delta t, \quad (3.6)$$

where the spatial derivatives are discretized by an upwind 5th order HJWENO scheme. Since the difference between ϕ^{n+1} and ϕ^n is very small, the difference of the mass enclosed by the zero level set curve between time level $n+1$ and n in discrete form can be expanded as

$$\begin{aligned} & \int_{\Omega} H_\varepsilon(\phi^{n+1}) dx - \int_{\Omega} H_\varepsilon(\phi^n) dx \\ & \approx \sum_{ij} (H_\varepsilon(\phi_{ij}^{n+1}) - H_\varepsilon(\phi_{ij}^n)) h^2 \\ & = \sum_{ij} \delta_\varepsilon(\phi_{ij}^n) (\phi_{ij}^{n+1} - \phi_{ij}^n) h^2 + \sum_{ij} \frac{H_\varepsilon''(\phi_{ij}^n)}{2} (\phi_{ij}^{n+1} - \phi_{ij}^n)^2 h^2 + \dots \end{aligned} \quad (3.7)$$

Since $\varepsilon \sim h$, we have $\delta_\varepsilon(\phi_{ij}^n) \sim \varepsilon^{-1} \sim h^{-1}$ and $H_\varepsilon''(\phi_{ij}^n) \sim \varepsilon^{-2} \sim h^{-2}$. In addition, formally we have $\phi_{ij}^{n+1} - \phi_{ij}^n \sim \mathcal{O}(\Delta t)$. Therefore, the first term in (3.7) is of order $h\Delta t$ and the second term is of the order $(\Delta t)^2$ when a standard level set method is used. On the other hand, when the constrained discrete equation (3.6) is used, the first term in (3.7) drops out, which in general reduces the discretization error. The discretization error can be further reduced when we use a smaller time step size, as indicated by the second term of (3.7).

In the implementation of the constrained level set method for the study of a complete liquid bridge formation process, the constraint equation (3.2) should be changed into

$$\frac{d}{dt} \left(\int_{\Omega} H(\phi) dx \right) = 2, \quad (3.8)$$

since the area occupied by displacing fluid increases with a constant rate 2 during the whole liquid bridge formation process, and a similar numerical method are implemented for the associated Lagrange multiplier

$$\lambda(t) = - \frac{2 + \int_{\Omega} \bar{u} \cdot \nabla \phi \delta(\phi) dx}{\int_{\Omega} \delta(\phi) dx}. \quad (3.9)$$

As we noted earlier, the idea of using Lagrange multiplier is not new. The new feature of our approach lies in the implementation of the method. For example, the constraint is not applied everywhere during the reinitialization stage in [2]. In this paper, we impose the constraint in each discretizations cell during reinitialization stage, following [3]. In addition, an upwind 5th order HJWENO scheme is used for spatial discretization. Consequently, our numerical results are more accurate than those in [3].

3.2 Discretization

The discretization used here is similar to that in [5]. We use staggered grids and ghost fluid method to compute the velocity and pressure fields. The level set method is used to capture the interface evolution. For more details we refer the readers to [5]. In our numerical implementation, the contact angle θ is assumed to vary smoothly from θ_1 to θ_2 in a thin layer along the patch boundary, instead of a jump across the boundary.

4 Results

Before solving the Hele-Shaw model for the liquid bridge problem, we tested the performance of the constrained level set method with its standard counterpart using two simple problems when velocity is given. The results, presented in Appendix B, show that the mass loss is much smaller for the constrained level set method. Furthermore, test results for the "Zalesak's disk" problem show that our HJWENO scheme is much more accurate than the finite element method [2]. Below we present numerical results for the liquid bridge problem.

4.1 Numerical results for a half-formed liquid bridge

In this section, we will compare the numerical results obtained by the constrained level set method and the asymptotic solutions. The setup and the asymptotic solutions are given in Appendix A.

Since 69° is the critical angle in patch region predicted by asymptotic approach for a half-formed liquid bridge, we set $\theta_2 = 69^\circ$ with other parameters taking the same values as in [1]. The final numerical interface profile is shown in Fig. 3 (black line), and the corresponding pressure values are plot in Fig. 4(a). The comparison between numerical calculated values of pressure jump across the interface (zero level set) and asymptotic values is given in Fig. 4(b). The comparison between our numerical calculated contact angle along the fluid interface (zero level set) and asymptotic value (i.e. 69°) is displayed in Fig. 5. Numerical computations are also carried out for $\theta_2 = 68^\circ$ and $\theta_2 = 70^\circ$. The results are shown in Fig. 3, where red line is the profile obtained by $\theta_2 = 68^\circ$ and green line corresponds to $\theta_2 = 70^\circ$.

From Fig. 3, it can be seen clearly that the final interface forms a half liquid bridge along the patch rim when $\theta_2 \leq 69^\circ$, while the half liquid bridge is formed inside the patch when $\theta_2 > 69^\circ$. These results confirm that the aforementioned conclusion that 69° is the critical value for formation of a half liquid bridge along the patch rim. Furthermore, Fig. 4(b) shows that maximum relative difference rate between numerical calculated values of pressure jump across interface and asymptotic values is less than 4%, and Fig. 5 shows that the numerical contact angles on the rim of patch fit the asymptotic values quite well. Thus, there are good quantitative agreements between numerical results and asymptotic solution for the static equilibrium state of a half-formed liquid bridge.

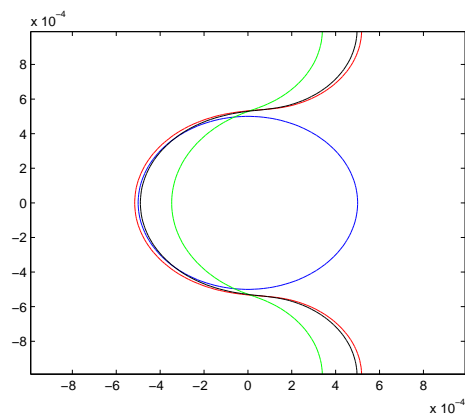
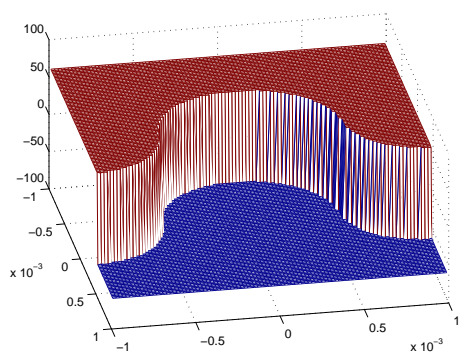
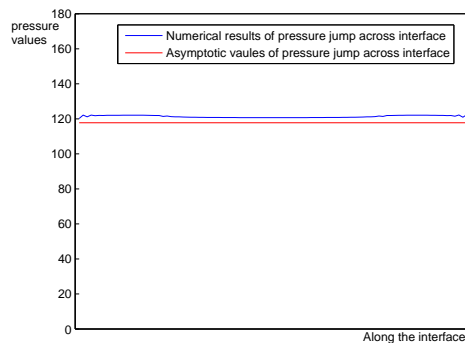


Figure 3: Numerical results using constrained level set method. Red line corresponds to $\theta_2 = 68^\circ$, black line corresponds to $\theta_2 = 69^\circ$, and green line corresponds to $\theta_2 = 70^\circ$. (Blue circle is the boundary of the wetting patch.)



(a)



(b)

Figure 4: (a): Plot of numerical calculated pressure. (b): Comparison between numerical calculated values of pressure jump across interface and asymptotic values.

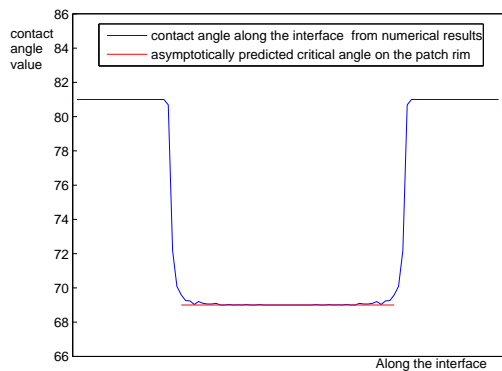


Figure 5: Comparison between numerical contact angle along the interface and asymptotically predicted critical contact angle on the patch rim.

4.2 Numerical results for the liquid bridge formation process

We now present the numerical results for the dynamic liquid bridge formation process using the constrained level set method. For comparison purpose, some numerical results obtained using the standard level set method are also presented.

In the first set of computations, we compare the results using standard level set method with that using constrained level set method. The parameter values used here are $\lambda = 0.005$, $\theta_1 = 81^\circ$, $\theta_2 = 45^\circ$, $Ca = 2.5 \times 10^{-4}$, $\eta = 1.2$, and the computations are carried out on 100×100 meshes. Fig. 6 shows the numerical solutions using both methods up to computational time $t = 1.7192$. It can be seen that the standard method suffers significant mass loss, as demonstrated by the reduction of the size of the liquid bridge. The constrained method, on the other hand, performs much better. In order to provide a clearer picture of the mass loss, we have computed the mass (projected area) of the liquid bridge for both methods, as shown in Fig. 7. It can be seen that the mass loss of the liquid bridge is significantly reduced for constrained level set method, compare to standard level set method. Furthermore, the mass of displaced fluid obtained by both methods are plotted to compare with the exact values, as shown in Fig. 8. It can also be seen that numerical displaced fluid area data fit the exact value well for the constrained level set method while it is not the case for the standard method after the formation of liquid bridge.

Other relevant physical quantities related to the liquid bridge formation process include the pressure field and streamlines. In Fig. 9, we plot the pressure and streamlines at two different stages of constrained level set method. It shows that pressure experiences large jump across the interface while the flow remains smooth. They also show that after the formation of the liquid bridge, pressure inside the liquid bridge is almost constant while outside a large pressure drop remains in the direction of the flow.

Next we study the effects of various physical and geometrical parameters have on the formation of liquid bridge. In all the computations, we use constrained level set method on a 100×100 mesh. The basic starting point for comparison is the case shown in Fig. 6(e-h). Fig. 10 gives the results based on the same parameter values as in Fig. 6 except the capillary number, which is increased to $Ca = 3.6 \times 10^{-4}$ from $Ca = 2.5 \times 10^{-4}$; Fig. 11 further increases Ca to $Ca = 3 \times 10^{-3}$; In Fig. 12, we changed viscosity ratio $\eta = 1.2$ to $\eta = 1.8$; and in Fig. 13 we further increase η to $\eta = 12$; In Fig. 14 we increased θ_2 to 58° instead of 45° ; Finally in Fig. 15 we further increase θ_2 to $\theta_2 = 75^\circ$.

These computations show that the formation of the liquid bridge is closely related to Ca which is a measure of the surface tension relative to the flow rate. When Ca is low, it is relatively easy for the interface to deform and subsequently the formation of the liquid bridge on the entire patch. When Ca increases, it becomes more difficulty to form the liquid bridge and a smaller one is formed. Increasing Ca further the interface sweeps through the patch area without forming the liquid bridge. The results also reveal the effect of viscosity ratio η between the two fluids. For smaller η , it is easier to form the liquid bridge while larger η makes it more difficult for the liquid bridges to form. The difference in contact angles between the hydrophilic and hydrophobic areas also has an

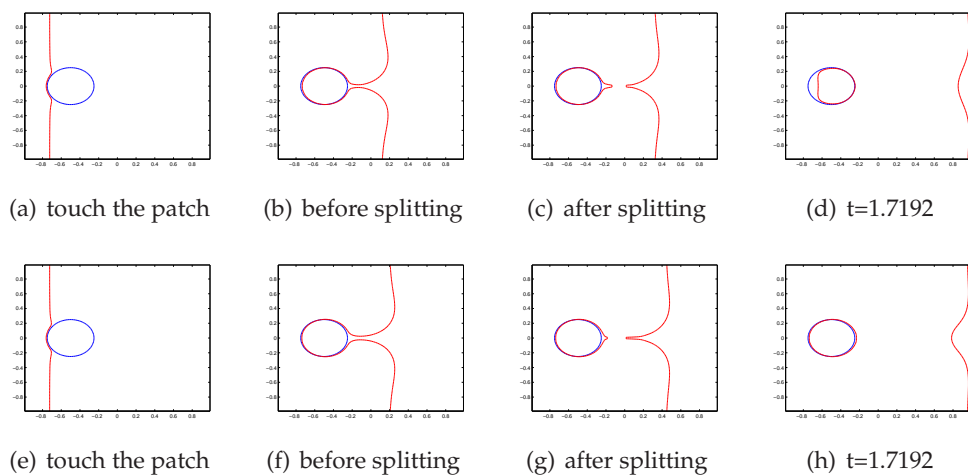


Figure 6: Numerical results obtained by using the standard level set method (a-d) and the constrained level set method (e-h). The parameter values are $\lambda = 0.005$, $\theta_1 = 81^\circ$, $\theta_2 = 45^\circ$, $Ca = 2.5 \times 10^{-4}$, $\eta = 1.2$.

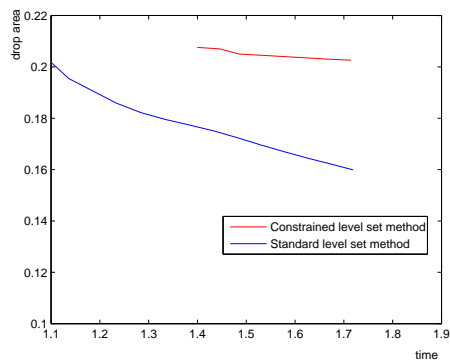


Figure 7: Time history of the liquid bridge mass (area) using constrained level set method and standard level set method

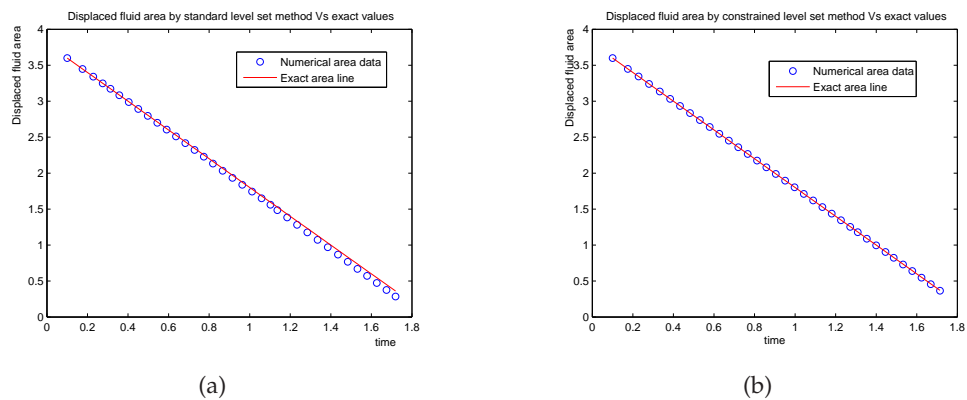


Figure 8: (a): Comparison between displaced fluid area by standard level set method and exact area line. (b): Comparison between displaced fluid area by constrained level set method and exact area line.

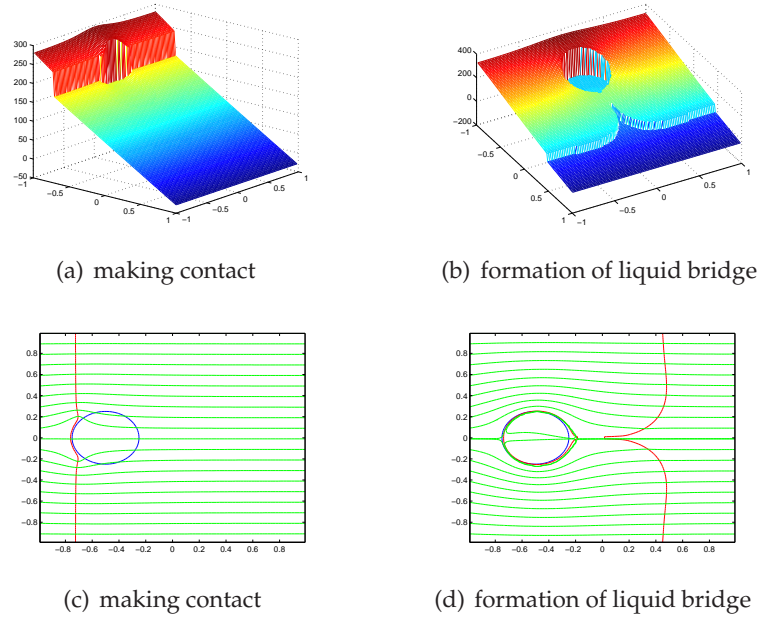


Figure 9: Pressure plots: (a) and (b); Streamlines: (c) and (d).

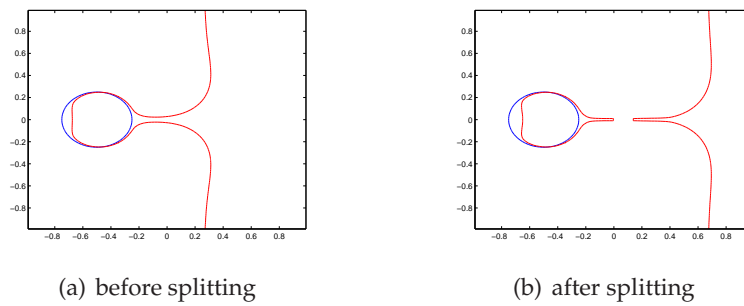


Figure 10: Numerical results by constrained level set method for $\lambda = 0.005$, $\theta_1 = 81^\circ$, $\theta_2 = 45^\circ$, $Ca = 3.6 \times 10^{-4}$, $\eta = 1.2$.

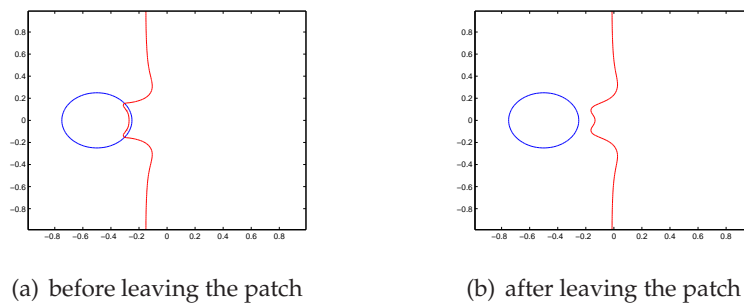


Figure 11: Numerical results by constrained level set method for $\lambda = 0.005$, $\theta_1 = 81^\circ$, $\theta_2 = 45^\circ$, $Ca = 3 \times 10^{-3}$, $\eta = 1.2$.

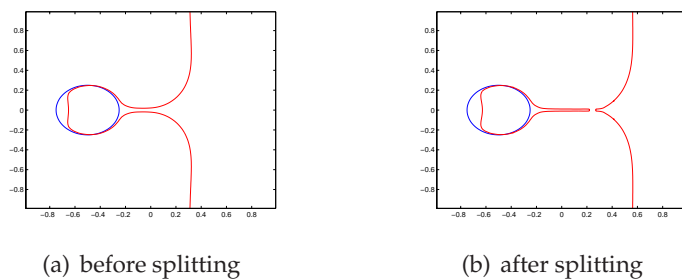


Figure 12: Numerical results by constrained level set method for $\lambda=0.005$, $\theta_1=81^\circ$, $\theta_2=45^\circ$, $Ca=2.5 \times 10^{-4}$, $\eta=1.8$.

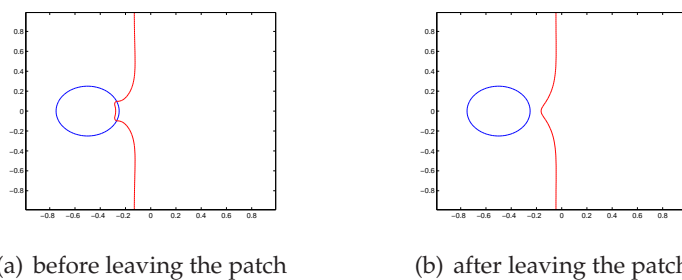


Figure 13: Numerical results by constrained level set method for $\lambda=0.005$, $\theta_1=81^\circ$, $\theta_2=45^\circ$, $Ca=2.5 \times 10^{-4}$, $\eta=12$.

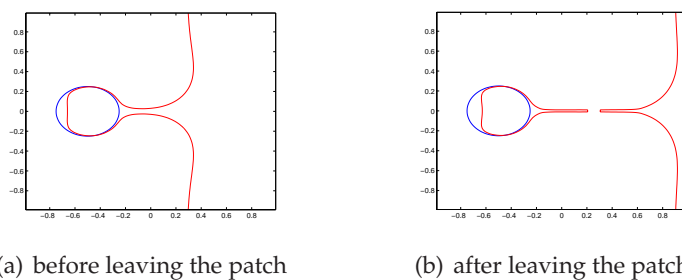


Figure 14: Numerical results by constrained level set method for $\lambda=0.005$, $\theta_1=81^\circ$, $\theta_2=58^\circ$, $Ca=2.5 \times 10^{-4}$, $\eta=1.2$.

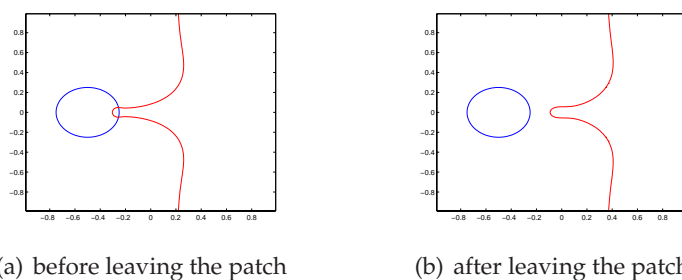


Figure 15: Numerical results by constrained level set method for $\lambda=0.005$, $\theta_1=81^\circ$, $\theta_2=75^\circ$, $Ca=2.5 \times 10^{-4}$, $\eta=1.2$.

effect. It is easier to form the liquid bridge when the difference in contact angle is large. All these are consistent with the experimental observations report in [1].

It is worth mentioning that the critical contact angle predicted by the asymptotic solution is $\theta_2 = 78^\circ$ based on the parameter values used in our computation. In other words, for any $\theta_2 \leq 78^\circ$, we would expect liquid bridges to form. Clearly, this is no longer true under the dynamic process, as demonstrated by our numerical simulation. In many cases, no liquid bridges or only partially formed liquid bridges are obtained despite the fact that θ_2 is far below the critical value.

5 Conclusions

In this paper, we apply a high order finite difference method (HJWENO) to solve the constrained level set evolution equation, which was first proposed by [2] in finite element context. We combine the above constrained evolution step with constrained reinitialization step [3] to form our constrained level set method. It is found that the constrained level set method reduce mass loss greatly through two standard test problems, and the method is much more accurate than the finite element method in [2]. We first use this method to simulate a half-formed liquid bridge and get good agreements with previous asymptotic results from [1]. Then we utilize both the constrained and standard level set method to simulate the dynamic formation process of a liquid bridge between two parallel plates with hydrophilic patches. Numerical results show that the constrained level set method is much better than the standard method, and also numerical predictions given by constrained level set method are consistent with the previous literature [1]. As a next step, we plan to carry out additional simulations for a multi-patch setup to examine the effect of neighboring patches by varying configurations of the patches. In addition, we also plan to improve our model by including the effect of the dynamic contact angle.

Acknowledgments

The authors would like to thank Robert M. Miura for bringing this problem to our attention and the participants of the BIRS FRG for helpful discussion. The work was supported by NSERC and MITACS (Canada). Computing resources provided by Sharcnet is also acknowledged.

A A Hele-Shaw model for formation of a half liquid bridge

Considering a half-formed liquid bridge as the static state and using the aspect ratio as a small parameter, authors in [1] derive asymptotic expressions for pressure jumps across

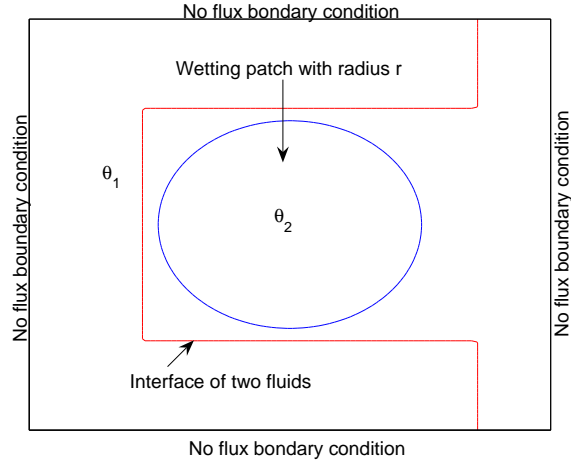


Figure 16: Computational domain and boundary conditions for a finally half-formed liquid bridge. Parameters are same as in [1]: $r = 5 \times 10^{-4} \text{m}$, $d = 1 \times 10^{-3} \text{m}$, $h = 5 \times 10^{-5} \text{m}$, $\theta_1 = 81^\circ$, $\sigma = 2.3 \times 10^{-2} \text{dyn/cm}$.

the interface in both the hydrophobic region and the patch rim region and as follows

$$[p]_1 = \frac{\sigma}{h} \left[\cos\theta_1 + \frac{\varepsilon_c}{2} \left(\frac{\frac{\pi}{2} - \theta_1}{\cos\theta_1} + \sin\theta_1 \right) + \dots \right],$$

$$[p]_r = \frac{\sigma}{h} \left[\cos\theta_r - \frac{\varepsilon_r}{2} \left(\frac{\frac{\pi}{2} - \theta_r}{\cos\theta_r} + \sin\theta_r \right) + \dots \right],$$

where $\varepsilon_c = \frac{h}{d-r}$, $\varepsilon_r = \frac{h}{r}$ and h is the half height between two plates, r is the patch radius, d is half distance between patch centers, σ is the interfacial tension between two fluids, θ_1 is the contact angle in hydrophobic region, θ_r is the contact angle on patch rim, $[p]_1$ is the pressure jump across interface in the hydrophobic region, and $[p]_r$ is the pressure jump across interface on the patch rim. By balancing these two jumps and using the parameters given in [1], we can give a criteria for formation of a half liquid bridge: $\theta_2 \leq 69^\circ \ddagger$, where θ_2 is the contact angle in the patch region.

To test our numerical method, we now set up a dynamic Hele-Shaw model with the half-formed liquid bridge as a possible final equilibrium state. The top view of the domain is shown in Fig. 16, where the initial interface can be chosen as any shape that cuts the domain into half, and parameters are the same as that in [1]. Since the gap between two plates is small compare to the size of the plate, we apply dimensional Hele-Shaw

[‡]This value is 56° in [1]. However, we believe this is a typo since we have verified the asymptotic solution in [1] and they do predict 69° as the critical value, furthermore, our numerical results also confirmed that the correct value is 69° .

equations for both fluids as follows [5]

$$\vec{u} = -\frac{h^2}{3\mu} \nabla p, \quad (\text{A.1})$$

$$\nabla \cdot \vec{u} = 0 \quad (\text{A.2})$$

for \vec{x} in Ω_+ and Ω_- with jump conditions

$$[p] = \sigma(\kappa_{xy} + \kappa_z), \quad (\text{A.3})$$

$$[\vec{u} \cdot \vec{n}] = 0 \quad (\text{A.4})$$

on Γ , where \vec{u} is velocity, μ is the dynamic viscosity, p is the pressure, Γ is the interface of two fluids, Ω_+ , Ω_- are the space occupied by displacing fluid and water, respectively, and κ_{xy} , κ_z are the dimensional curvature in the xy and z plane respectively, and

$$\kappa_z = -\frac{\cos\theta}{h} \quad (\text{A.5})$$

using the same assumption in Section 2, and θ is the contact angle, and $\theta = \theta_1$ in all the computational domain except the patch region where $\theta = \theta_2 < \theta_1$.

For the computations, we choose three connected straight lines which are showed in Fig. 16 as the initial interface of two fluids and use no flux boundary conditions here.

B Additional numerical tests

Here we provide the results when the standard and constrained level set methods are applied two standard test problems. In both cases, velocity fields are given and the zero level set of a function evolves according to the velocity fields.

B.1 Zalesak's disk

We consider a unit square computational domain with a rigid body rotation [8] $u = 0.5 - y$ and $v = x - 0.5$. Initially, the zero level set represents a slotted circle centered at $(0.5, 0.75)$ with a radius of 0.15, a width of 0.05, and a slot length of 0.25. We use both standard and constrained level set methods to calculate the problem. The mass of the disk is calculated through $\int_{\Omega} H_{\varepsilon}(\phi) dx$ and its associated regularized form (3.5).

The numerically computed zero level sets after one rotation are presented in Fig. 17 for the standard and constrained level methods. The relative mass loss after one revolution and convergence rates are given in Table 1. The results clearly show that the constrained level set has better mass conservation property than the standard one, especially when on relatively coarse grids. Furthermore, our results show that the HJWENO scheme is 5th order accurate, however, the results for the same problem in [2] is only 0.5 order accurate, mass loss of our result for a resolution 100×100 is less than 0.3%, even better than the results obtained by 400×400 meshes in [2], we can conclude that the HJWENO scheme is much more accurate than the finite element method.

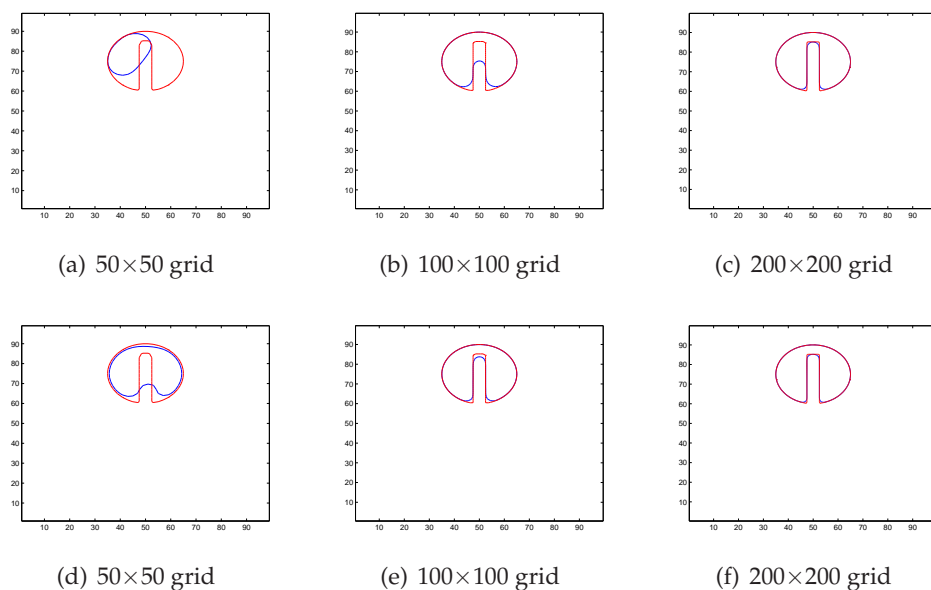


Figure 17: Results using standard level set method (a-c) and results using constrained level set method (d-f). The red line is the exact solution, and the blue line is the numerical solution.

Table 1: Zalesak's disk: Relative mass loss (%) and convergence rate using standard level set method and the constrained level set method.

Grid Size	Standard	Convergence rate	Constrained	Convergence rate
50×50	55.6	-	3.84	-
100×100	-4.86	3.516	0.29	3.727
200×200	0.38	3.6769	0.0116	4.6439

B.2 Single vortex

To further compare the performance of the standard and constrained level set methods, we use the following velocity field on a unit square: $u = \sin^2(\pi x)\sin(2\pi y)$ and $v = -\sin^2(\pi y)\sin(2\pi x)$ for $0 \leq t \leq T$. The zero levelset is a circle with radius 0.15, initially centered at (0.5,0.75). This velocity field is reversed at time $t = T$ so that the zero levelset at $t = 2T$ coincides with the initial condition.

Previous literature (see [9]) shows that the best result by level set method for this problem is obtained without reinitialization. Therefore, we use standard level set method and constrained level set method without reinitialization. We choose $T = 4$ in the computation so that the maximum deformation happens when $t = 4$ and the exact solution at $t = 8$ should coincide the initial condition.

The numerical result of the standard level set method on a 256×256 grid is given in Fig. 18 while the result using the constrained level set method on the same grid is presented in Fig. 19.

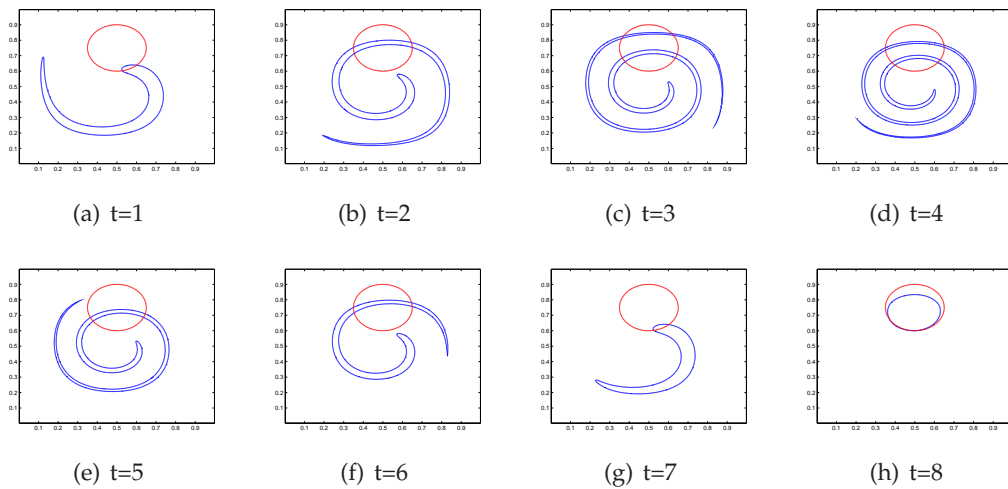


Figure 18: Numerical simulation by standard level set method without reinitialization using 256×256 meshes. (The red line is the initial circle, and the blue line is numerical solution).

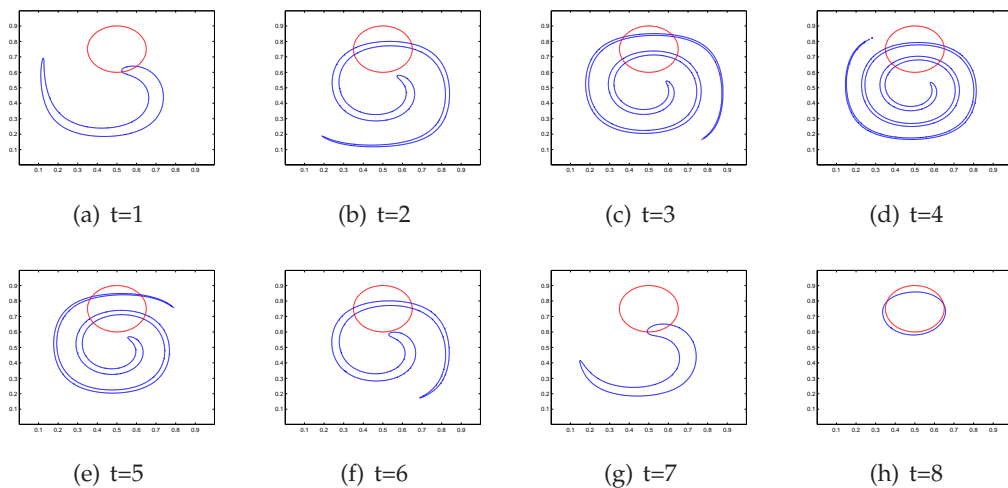


Figure 19: Numerical simulation by constrained level set method without reinitialization using 256×256 meshes. (The red line is the initial circle, and the blue line is numerical solution).

To quantify mass conservation, we use two measures. In the first case we compute the mass using the regularized form, i.e., integral $\int_{\Omega} H_{\varepsilon}(\phi) dx$ and its associated regularized form (3.5) and the relative mass loss is given in Table 2. In the second case, the mass is computed by the integral $\int_{\Omega} H(\phi) dx$ without regularizing $H(\phi)$. The relative mass loss is given in Table 3. Once again, the constrained level set method outperforms the standard one, no matter which mass measure method is used.

Table 2: Single vortex: relative mass loss (%) using the standard and constrained level set methods based on the regularized Heaviside mass measure.

Grid Size	Standard	Constrained
128×128	79.96	0.01863
256×256	29.48	0.00961
512×512	4.93	0.00785

Table 3: Single vortex: relative mass loss (%) using the standard and constrained level set methods based on the Heaviside mass measure.

Grid Size	Standard	Constrained
128×128	80.78	1.21
256×256	29.60	0.48
512×512	5.04	0.18

References

- [1] J. Silver, Z. Mi, K. Takamoto, P. Bungay, J. Brown and A. Powell, Controlled formation of low-volume liquid pillars between plates with a lattice of wetting patches by use of a second immiscible fluid, *J. Colloid. Interf. Sci.*, 219 (1999), 81-89.
- [2] A. Laadhari, P. Saramito and C. Misbah, Improving the mass conservation of the level set method in a finite element context, *C. R. Acad. Sci. Paris, Ser. I.*, 348 (2010), 535-540.
- [3] M. Sussman and E. Fatemi, An efficient, interface-preserving level set redistancing algorithm and its application to interfacial incompressible fluid flow, *SIAM J. SCI. Comput.*, 20 (1999), 1165-1191.
- [4] M. Sussman, P. Smereka, and S. Osher, A level set method approach for computing solutions to incompressible two-phase flow, *J. Comput. Phys.*, 114 (1994), 146-159.
- [5] D. He, H. Huang and Y. Tan, Numerical simulation for a droplet fission process of electrowetting on dielectric device, *Commun. Comput. Phys.*, 7 (2010), 1076-1094.
- [6] T. Hou, Z. Li, S. Osher and H. Zhao, A hybrid method for moving interface problems with application to the Hele-shaw flow, *J. Comput. Phys.*, 134 (1997), 236-252.
- [7] G. Jiang and D. Peng, Weighted ENO schemes for Hamilton-Jacobi equations, *SIAM J. SCI. Comput.*, 21 (2000), 2126-2143.
- [8] S. Zalesak, Fully multidimensional flux-corrected transport algorithms for fluids, *J. Comput. Phys.*, 31 (1979), 335-362.
- [9] P. Gómez, J. Hernández and J. López, On the reinitialization procedure in a narrow-band locally refined level set method for interfacial flows, *Int. J. Numer. Meth. Eng.*, 63 (2005), 1478-1512.